Composite Structures 133 (2015) 131–139

Contents lists available at ScienceDirect

Composite Structures

journal homepage: www.elsevier.com/locate/compstruct

Effects of bonding in short-span rectangular concrete filled GFRP tubes

M.J. Robinson *, I.H. Melby

Civil and Environmental Engineering, South Dakota School of Mines and Technology, Rapid City, SD 57701, United States

ARTICLE INFO

Article history:
Available online 23 July 2015

Keywords:
Composite
Tube
Concrete-filled
Bonding
Beam
Finite element

ABSTRACT

Flexural performance of concrete-filled tubes is highly dependent on the composite action between the concrete core and encasing tube. This study investigates the performance of short-span concrete-filled rectangular glass fiber reinforced polymer (GFRP) tubes with different levels of bonding between the concrete core and GFRP tube. The bonding configurations include (1) no bonding, (2) bonding of the webs, (3) bonding of the flanges, and (4) bonding of the webs and flanges. The study includes both experimental and finite element analysis results for each configuration. Comparing the performance of each configuration showed a two fold increase in stiffness and strength as a result of bonding between the concrete core and GFRP tube. Furthermore it was concluded that bonding of the flanges was most critical with web bonding providing only a slight increase in performance.

1. Introduction

Concrete-filled glass fiber reinforced polymer (GFRP) tubes represent an efficient structural building element having several advantages over conventional reinforced concrete elements. The GFRP tube acts as stay-in-place formwork, greatly reducing construction cost and time as well as serving as external reinforcement eliminating the need for internal steel reinforcement [1,9]. In addition, the GFRP tube may provide concrete confinement as well as increased resistance to degradation in corrosive environments. Although many studies have been performed for circular concrete-filled GFRP members in both axial and flexural applications [4], much less attention has been given to concrete-filled rectangular sections, particularly beams utilizing pulturded sections.

Fam et al. [6] investigated rectangular filament wound concrete filled tubes with combined axial and flexural loading. Fam and Skutezky [7] studied T-beams constructed of concrete-filled rectangular GFRP pultruded beams with concrete slabs attached with shear studs. As part of this study, a comparison of concrete filled and non-filled GFRP tubes showed little additional stiffness but a large increase in strength due to the presence of the concrete core. Conversely, a comparison of concrete-filled and non-filled GFRP tubes with the addition of the concrete deck showed a large increase in stiffness but only slight increase in strength. Honickman and Fam [11] developed a hybrid trapezoidal box girder utilizing pultruded GFRP sheet piling filled with concrete and capped with a concrete deck. Results from this study found the bond between the concrete and GFRP sheet material to be the limiting factor for the ultimate strength of the girder system. Chakrabortty et al. [3] developed a hybrid concrete-FRP beam consisting of a pultruded GFRP tube with high strength concrete placed on the top flange and a CFRP laminate bonded to the lower flange. The assembly was then encased within a GFRP filament wound laminate. The concrete and CFRP laminate significantly increased the flexural stiffness and strength of the beam with the filament wound outer laminate providing confinement of the concrete flange as well as increasing the shear stiffness and strength. Shawkat et al. [15] investigated short-span concrete-filled pultruded GFRP tubes with and without steel reinforcing. Based on concrete cracking patterns it was noted that unreinforced specimens primarily exhibited flexural cracking while reinforced specimens showed a combination of flexure and shear cracking. Most recently, Belzer et al. [2] investigated the effects of bonding between the concrete core and pultruded GFRP tubes for long-span rectangular beams. The results showed full composite action for completely bonded specimens with only partial composite action for cases where only the flanges were bonded. The difference in shear response between the fully bonded specimens and those with only the flanges bonded was notable. Based on these results the current research expands the previous research of Belzer et al. [2] to investigates short-span specimens where displacements due to shear are significant. This is accomplished through three-point bend testing of short-span concrete-filled beams with different levels of bonding between the concrete core and GFRP tube. Examination of the experimental displacement and

* Corresponding author. Tel.: +1 (605) 394 2563.
E-mail addresses: marc.robinson@sdsmt.edu (M.J. Robinson), ivarmelby@gmail.com (I.H. Melby).

http://dx.doi.org/10.1016/j.compstruct.2015.07.105
0263-8223/

strain results as well as analytical results for each configuration is used to assess performance.

2. Experimental

The experimental portion of this work consists of a description of the test specimens including material properties, fabrication methods, and experimental test setup.

2.1. Test specimens

Four different concrete core-to-tube bonding configurations as well as empty tubes were tested. As shown in Fig. 1, the different configurations consist of empty tubes (A), no bonding (B), bonding to webs (C), bonding to flanges (D), and bonding to webs and flanges (E). For each configuration three specimens were tested for a total of 15 beams. The tubes had a depth of 203 mm and a width of 152 mm with a flange and web thicknesses of 9.5 mm and 6.4 mm respectively (Fig. 1). The beams were tested using a simple span of 710 mm resulting in a span-to-depth ratio (L/d) of 3.5.

The concrete-filled specimens were fabricated by coating the appropriate interior surfaces of the tubes with a wet cure epoxy immediately prior to concrete placement. The tubes were placed on end and a funnel was used to prevent concrete running down the sides of the tubes eliminating any potential for epoxy washout. The bottom ends of the tubes were capped to contain the concrete. Illustrations of the fabrication process are shown in Fig. 2. The concrete was allowed to cure for a minimum of 40 days prior to testing.

2.2. Materials

The specimens consist of a concrete core, GFRP tube, and wet cure epoxy. To minimize voids within the specimens, a highly flowable concrete mix design having a target strength of 44.8–51.7 MPa was used. Mix proportions for the concrete are given in Table 1. Concrete cylinders tested in parallel with the beam testing showed the concrete to have an average strength of 48 MPa.

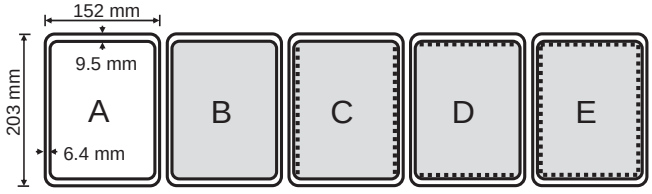

Fig. 1. Illustration of test specimen configurations (A) empty, (B) unbonded, (C) webs bonded, (D) flanges bonded, and (E) flanges and webs bonded.

Table 1
Concrete mix design.

Material	Quantity/m^3
Cement	309 kg
Fly ash	77 kg
Coarse aggregate	792 kg
Intermediate aggregate	221 kg
Fine aggregate	702 kg
Air-entraining admixture	387 mL
Water reducer (Pozzolith 322N)	5.8 L
Water reducer (Polyheed)	7.9 L
Air content	6.5%

Table 2
GFRP tube mechanical properties.

Location (Orientation)	Strength MPa	Failure Strain	Modulus GPa	Poisson's ratio
Flange (L*)	378.0	0.0155	27.6	0.29
Flange (T*)	72.4	0.0144	8.6	0.09
Web (L)	355.0	0.0166	23.8	0.28
Web (T)	71.5	0.0128	8.0	–
Web (S*)	37.2	–	0.5	–

*L-Longitudinal, T-Transverse, S-Shear.

The GFRP tubes were commercially available pultruded rectangular sections from EVAPCO. The laminates consist of polyester resin with longitudinal E-glass roving layers separated by high melt polyester veil mats. The flanges contain three longitudinal E-glass plies interspersed with five polyester veil mats and the webs consist of two longitudinal E-glass plies interspersed with three polyester veil mats. Mechanical testing of the webs and flanges were performed to obtain both longitudinal and transverse material properties. A summary of the material properties is given in Table 2.

The epoxy (Product #7 from Epoxy.com) used to bond the concrete to the GFRP tube co-cures with wet concrete. Product #7 is a two part epoxy mixed at a 1:1 ratio by volume. A summary of material properties provided by the manufacturer are given in Table 3. Double lap shear tests showed the bond strength of the epoxy to the GFRP laminate to be 4.0 MPa. Based on previous studies [10,14], as well as post mortem inspection from this research, it was observed that the failure always occurred in the concrete layer and never in the bond between the epoxy and GFRP laminate.

2.3. Test setup

The specimens were tested in three-point bending as shown in Figs. 3 and 4. The ends were supported on pins with a 152 × 152 × 25 mm steel plate with 3 mm thick rubber pad to prevent local failure of the GFRP tube. The load was also applied through a steel plate and rubber pad of the same dimensions to

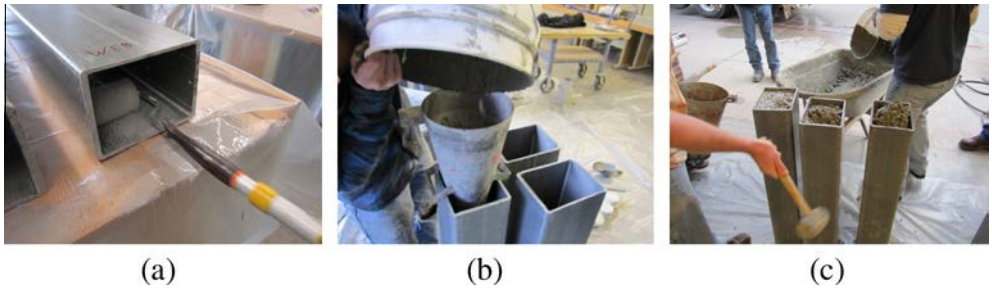

Fig. 2. Illustrations of (a) epoxy placement, (b) concrete placement, and (c) consolidation.

Table 3
Product #7 epoxy properties.

Property	Measure
Modulus of elasticity	3792 MPa @ 28 days
Bond strength	13.8 MPa @ 14 days
Tensile strength	41.4 MPa @ 7 days
Flexural strength	51.7 MPa @ 14 days
Compressive strength	69.0 MPa @ 7 days
Viscosity	6000 cps
Tack free time	6 h @ 15.6 °C 3 h @ 24 °C 1 h @ 90 °C

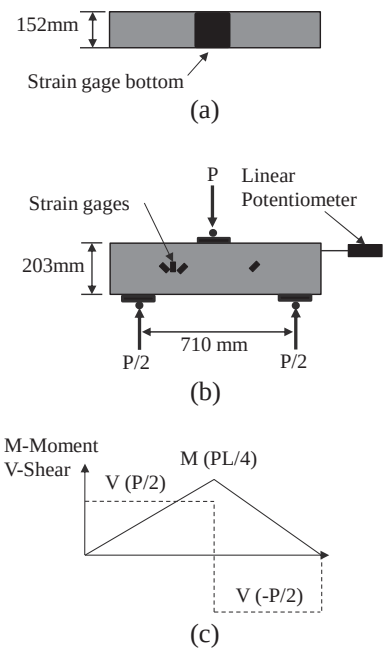

Fig. 3. Schematic of three point bend test setup with instrumentation: (a) top view; (b) side view; (c) corresponding shear and moment diagrams.

Fig. 4. Photograph of beam specimen under three point bending.

distribute the point load. A strain gage rosette was located mid-way between the support at one end and the mid-span to measure the shear strain. An additional gage between the other support and mid-span was oriented at 45° to confirm the shear strain measurements were symmetric. A strain gage was located on the bottom flange at the mid-span to record maximum bending strains. A linear potentiometer located at one end of the specimen was used to measure the relative displacement (slipping) between the concrete core and GFRP tube. Each specimen was loaded at a displacement rate of 0.64 mm/min. A diagram of the shear and moment profiles produced by the test setup is given in Fig. 3c.

3. Analytical

In addition to the experimental measurements an analytical study was performed to provide further insight into the experimental results. The study includes the use of conventional Timoshenko Beam Theory [8] as well as finite element modeling.

3.1. Timoshenko Beam Theory

The empty tubes (A) and unbonded configuration (B) were modeled using Timoshenko Beam Theory given by

$$v = \frac{PL^3}{48EI} + \frac{PLf_s}{4GA}, \tag{1}$$

where v is the displacement at the mid-span, P is the load, L is the span, E is the longitudinal modulus of the GFRP shell, I is the moment of inertia of the empty tube, G is the in-plane shear modulus of the GFRP tube webs, A is the cross section area, and f_s is the form factor which is dependent on the cross section geometry. For the case of the empty tube the form factor is calculated as the total cross section area divided by the area of the webs and is found to be 2.24.

3.2. Finite element modeling

For the bonded configurations (C, D, and E) finite element models were created and analyzed using ABAQUS/Explicit 6.12. Based on the symmetry of the specimens the model is reduced to 1/4 of the total specimen dimensions as shown in Fig. 5. A plane of symmetry is defined at the mid-span as well as along the centerline of the beam. The load is applied as a pressure over the area of the steel loading plate and a roller support condition is applied at the end support. The mesh consists of four-node quadrilateral elements.

Three different models were created to model the different bonding conditions. As seen in Fig. 6 the models for conditions C and D include finite gaps in the mesh along the flanges and web respectively. Within these gaps contact surfaces are created in ABAQUS such that the concrete and GFRP mesh surfaces cannot penetrate each other providing out-of-plane support to the GFRP tube and preventing buckling. More information on defining contact surfaces in ABAQUS can be found in the User's Manual [5]. For configuration E the mesh between the core and GFRP is continuous.

In order to capture the effects of concrete cracking of the core the *concrete damaged plasticity* model was used [5]. The material parameters used in the model are given as follows:

- dilation angle, $\psi = 31$
- flow potential eccentricity, $m = 0.1$
- initial biaxial/uniaxial ratio, $\sigma_{c0}/\sigma_{b0} = 1.16$
- ratio of 2nd stress invariant on the tensile meridian, $K_c = 0.67$
- viscosity parameter, $\mu = 0$

The dilation angle is a typical value for concrete modeling based on Nielsen and Hoang [13] and the other parameters are ABAQUS default values for the *concrete damaged plasticity* model.

Compressive and tensile stress versus strain constitutive data were adopted from Jankowiak and Tomasz [12]and are given in Tables 4 and 5 respectively. The data is a result of experimental measurements for class B50 concrete having a peak strength of 50 kPa and provides compressive (Table 4) and tensile (Table 5) stress versus strain relationships for the concrete beyond the linear elastic range. Based on peak strength the data corresponds well with the concrete used in this study.

4. Results and discussion

The experimental measurements and analytical results are presented for each beam configuration. The results include a comparison of the strength and stiffness of each configuration, slip between the core and tube, shear response, and finally observed failure modes.

4.1. Load–displacement

Plots of load versus displacement for each configuration along with analytical or finite element (FE) results are given in Fig. 7. From Fig. 7a it is seen that the theoretical displacement based on Eq. (1) agrees well with the experimental results. It is also observed that the displacement of the empty GFRP tube is dominated by shear deformation (73% of deflection is due to shear). Fig. 7b shows that for configuration B once initial flexural cracking occurs that the stiffness of the specimens approaches that of the empty tube solution with the concrete core providing minimal stiffness. This is confirmed from the load versus slip results shown in Fig. 8.

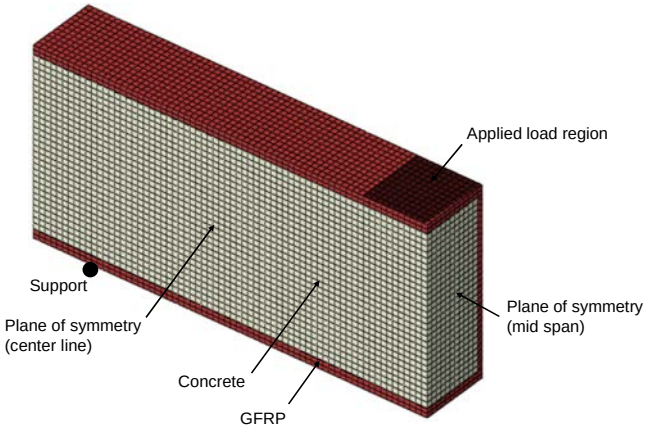

Fig. 5. Finite element model showing boundary and loading conditions.

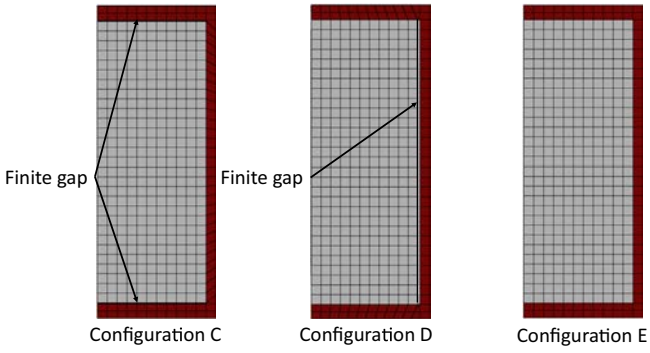

Fig. 6. Finite element models of mid-span cross section showing mesh for each configuration.

From the plot it is observed that slip between the core and GFRP tube initiates at approximately 30–40 kN and continues through the test indicating a loss of composite action. Load displacement plots for bonded configurations C, D, and E are given in Fig. 7c and d, and e respectively. From the plots it is seen that the FE results show very good agreement with the experimental measurements. From Fig. 7c it is observed that the displacement response for each specimen shows an abrupt change in stiffness due to bond failure between the concrete core and GFRP webs. This is confirmed by the slip measurements from Fig. 8 where it is seen that slip occurs at approximately 75 kN, 120 kN, and 145 kN corresponding to the abrupt changes in stiffness. This is further confirmed by the measured shear strain responses presented in the following section. It should be noted from Fig. 8 that for specimens C-1 and C-2 the slip abruptly goes negative when the bond fails and then trends back to positive following concrete failure. This is best illustrated in Fig. 9 where it is shown that under bending conditions there is no slip between the concrete and GFRP tube prior to bond failure (Fig. 9a) with a negative slip occurring when composite action is lost due to bond failure (Fig. 9b) and finally a positive slip after the concrete fails in bending and the concrete core begins to push out of the GFRP tube (Fig. 9c). For configuration D (Fig. 7d) it is seen that there is a slight decrease in stiffness for all of the specimens when flexural cracking occurs (≈30–40 kN) followed by a second decrease which occurs at 150 kN for D-3 up to 250 kN for D-1. This is likely due to some debonding of the flanges which is not included in the FE model. Similarly Configuration E shows a change in stiffness resulting from flexural cracking with E-3 showing a discontinuity at 200 kN which again is likely due to debonding.

A comparison of all five specimen types is shown in Fig. 7f along with a summary of the average strength and stiffness of each given in Table 6. For comparison purposes each configuration has been normalized with respect to configuration B (unbonded). For configurations B through E the stiffness is based on the deflection at a load level of 70 kN which is greater than the flexural cracking load but less than the failure load. For configuration A a load of 50 kN is used. It is observed from the table that while configuration B has more than twice the strength of A, the stiffness is only slightly higher as explained previously. Bonding of the webs (C) showed a significant increase in stiffness however only a slight increase in strength due to bond failure between the core and webs. Configurations D and E showed significant increases in both strength and stiffness with configuration E having twice the strength and stiffness of B.

Finite element analysis plots of the longitudinal stress contours for configurations C through E are given in Fig. 10. The stress plots are the result of a 160 kN load (approximate failure load for configuration C) where each plot used the same contour scale for comparison purposes. A comparison of FE results and experimental measurements are given in Table 7 where it is noted that the FE model showed good agreement with the measurements. From Fig. 10 it is seen that the longitudinal stresses in the flange and web vary for each configuration where D (Fig. 10b), which has only the flange bonded, shows the highest stresses and C (Fig. 10a), which has only the webs bonded, gives the lowest stresses. Configuration E (Fig. 10c) has both webs and flanges bonded and shows a stress state which is between configurations C and D.

4.2. Shear

In addition to load–displacement, shear response is also investigated. Fig. 11 gives the shear strain as a function of shear load for each configuration. From Fig. 11a it is observed that following flexural cracking configurations A and B show near identical responses. Furthermore, following debonding of the webs,

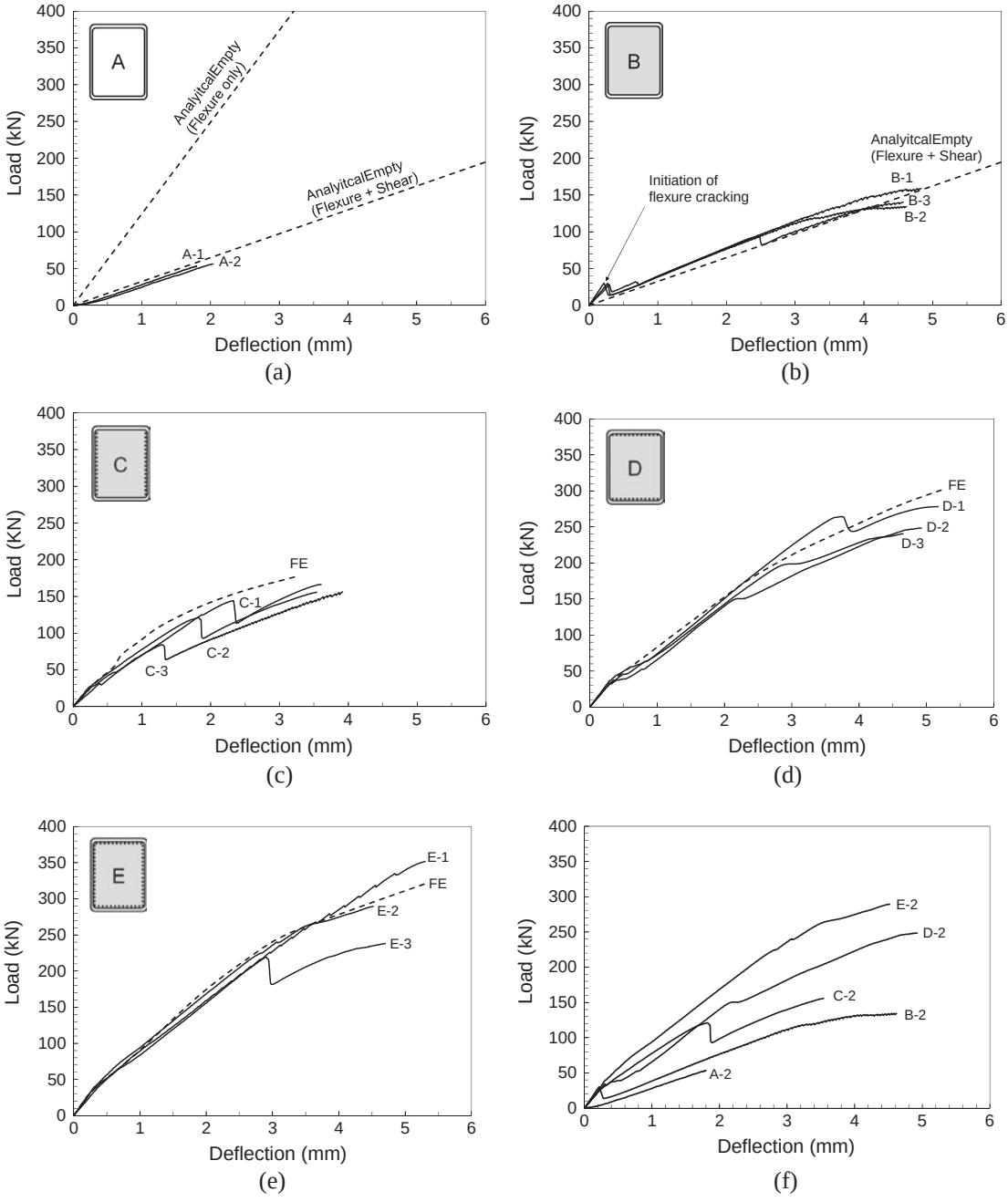

Fig. 7. Load deflection plots for (a) empty, (b) unbonded, (c) bonded webs, (d) bonded flanges, (e) bonded webs and flanges, and (f) comparison of all configurations.

Table 4
Compressive behavior.

Yield stress (MPa)	Inelastic strain
15.0	0
20.0	0.0000747
30.0	0.0000988
40.0	0.000154
50.0	0.000762
40.0	0.00256
20.0	0.00568
5.3	0.0117

Table 5
Tensile behavior.

Yield stress (MPa)	Cracking strain
2.00	0
2.84	0.0000333
1.87	0.000160
0.86	0.000280
0.23	0.000685
0.06	0.00109

configuration C shows the same response as configurations A and B. This confirms that the discontinuity in the load–displacement from Fig. 7c is due to web debonding. Experimental results for configurations D and E are given in Fig. 11b. From these results it is observed that configuration E follows a similar response to configuration C where the curve is very steep and then drastically

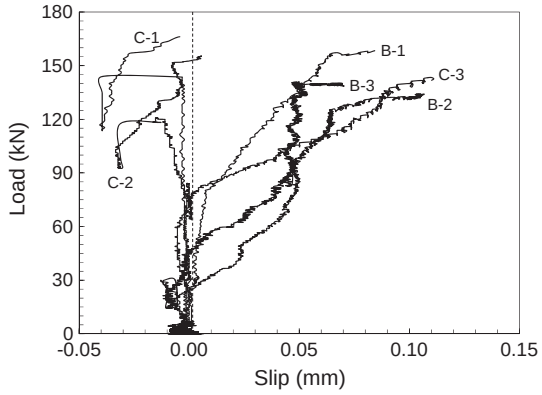

Fig. 8. Plot of load versus concrete core slip for configurations B and C.

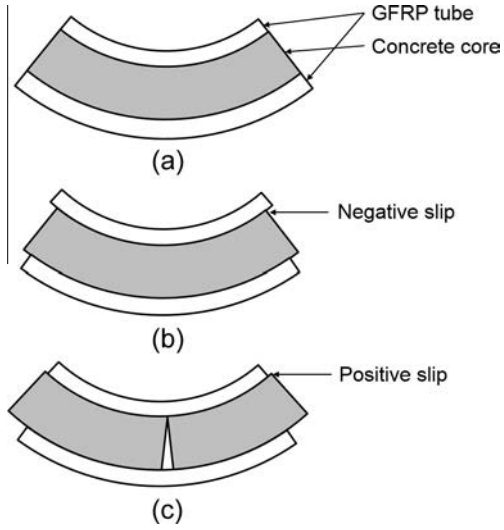

Fig. 9. Illustrations of (a) composite action with no slipping, (b) non-composite action with negative slipping and (c) non-composite action with concrete failure and positive slip.

decreases at a shear value near 40–50 kN suggesting debonding of the webs. However due to the flange bonding the shear load continues to increase up to final failure. Configuration D shows a slight reduction in shear stiffness following flexural cracking at which point it continues at lower shear stiffness up to failure.

A comparison of the finite element results with experimental measurements for configurations C through D are given in Fig. 12. From the plots it is seen that the finite element models show reasonable agreement with measurements but are not able

Table 6
Short beam strength and stiffness ratios.

Specimen	P_{ult} (kN)	Avg (kN)	Strength ratio	SD	K (kN/mm)	Avg (kN/mm)	Stiffness ratio	SD
A-1	50				31			
A-2	53	52	0.4	2.2	30	31	0.8	0.6
A-3	–				–			
B-1	158				39			
B-2	133	144	1.0	12.8	38	39	1.0	0.4
B-3	141				39			
C-1	166				69			
C-2	155	159	1.1	6.1	77	71	1.8	5.4
C-3	156				67			
D-1	278				74			
D-2	249	256	1.8	19.9	67	73	1.9	5.6
D-3	240				78			
E-1	351				93			
E-2	289	293	2.0	56.6	101	79	2.0	8.1
E-3	238				85			

Table 7
Bottom flange strains (90 kN load).

Configuration	C	D	E
Experimental strain	0.00120	0.00136	0.00127
FE strain	0.00113	0.00128	0.00116
% error	−6%	−6%	−9%

to capture the effects of debonding. In-plane shear contour plots for configurations C through D at a load level of 160 kN are given in Fig. 13. From the contour plots it is seen that configuration C shows significantly higher shear strains in comparison to configurations D and E. The bonding of the flanges for configurations D and E allow the shear forces to transfer directly into the concrete while configuration C requires the shear to be transferred through the webs resulting in significantly higher shear strains.

4.3. Failure

Inspection of the specimens following failure revealed two common failure modes which are illustrated in Fig. 14. Configuration A failed in punching shear of the top flange at the location of loading while configurations B through D showed tension failure of the web-flange interface along the bottom center of the beams and at the top web-flange interface over the supports. This same failure mode was observed by Shawkat et al. [15] and is confirmed through modeling as shown in Fig. 14c. Once web bonding is lost and significant concrete cracking has occurred, shear capacity of the concrete is diminished and the load is transferred

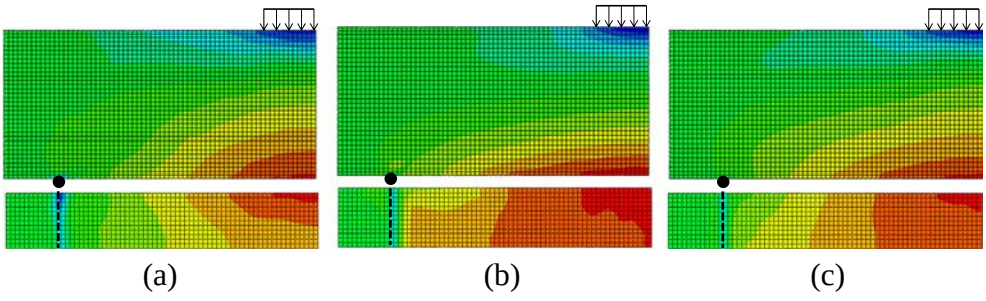

Fig. 10. GRRP longitudinal stress of web and bottom flange at a load of 160 kN for configurations (a) C, (b) D, and (c) E. All contour plots share a common scale.

by the concrete directly to the bottom flange at the mid-span. Likewise the reaction forces are transmitted to the top flange leading to the observed failures.

The *concrete damaged plasticity* model is used to predict crack patterns in the concrete core for configurations C, D, and E as shown in Fig. 15. From the figure it is observed that configurations D and E (Fig. 15b and Fig. 15c) show similar cracking patterns which are consistent with shear failure while configuration C (Fig. 15a) showed discrete cracks more representative of flexural cracking. At low loads all three models show initial flexural cracking occurring at the mid-span. Photographs of the cracking patterns of each configuration are given in Fig. 16. From the photos it is observed that configuration B shows a single flexural crack at the mid-span of the beam while C and D show additional cracking either side of the mid-span. Configuration E exhibits a cracking pattern which is more consis-

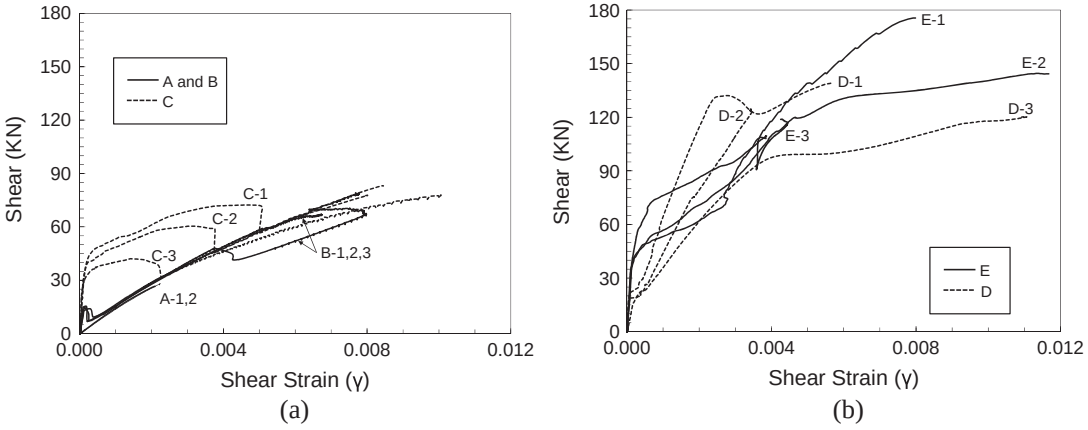

Fig. 11. Plot of shear versus strain for configurations (a) A, B, and C, and (b) D and E.

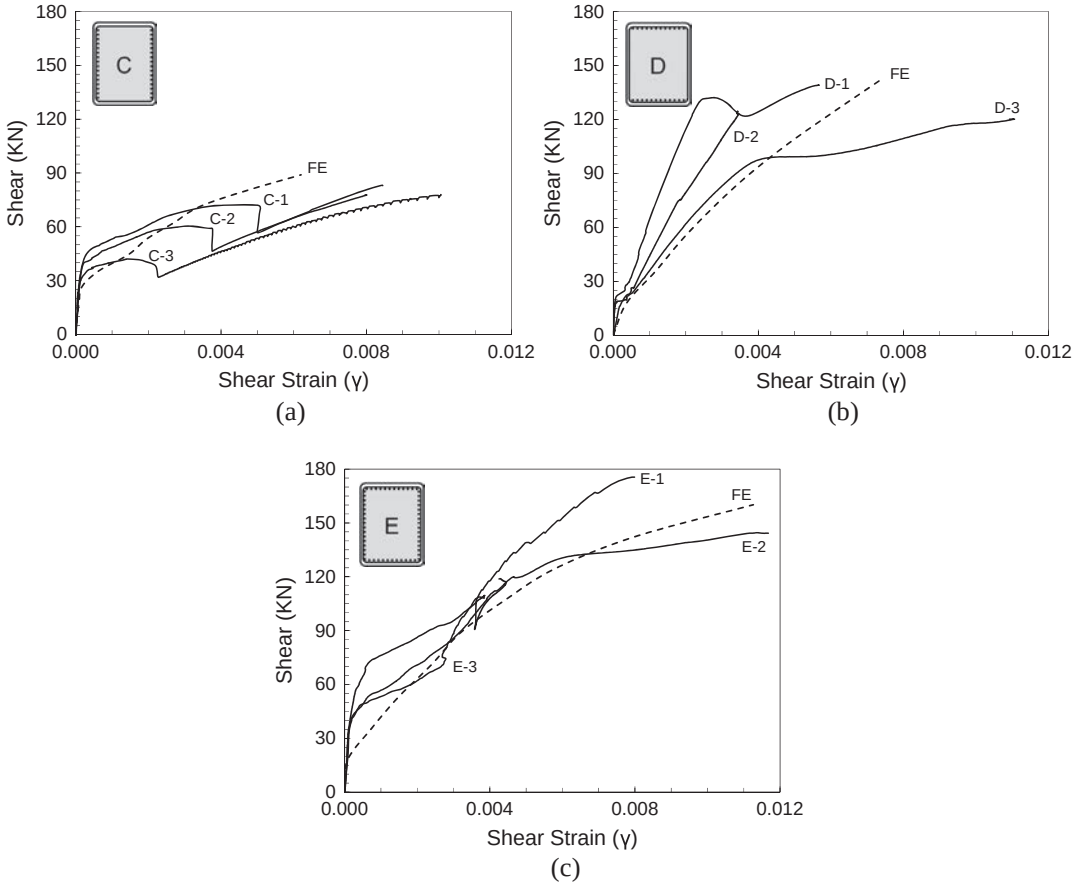

Fig. 12. Plots of shear versus strain of configurations (a) C, (b) D, and (c) E.

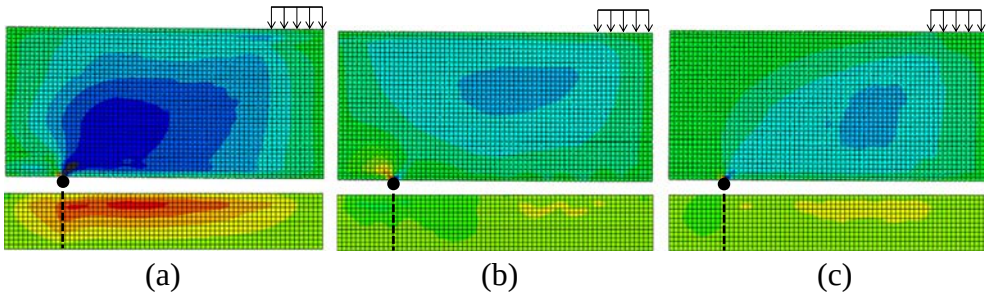

Fig. 13. GRRP in-plane shear strain of web and bottom flange at a load of 160 kN for configurations (a) C, (b) D, and (c) E. All contour plots share a common scale.

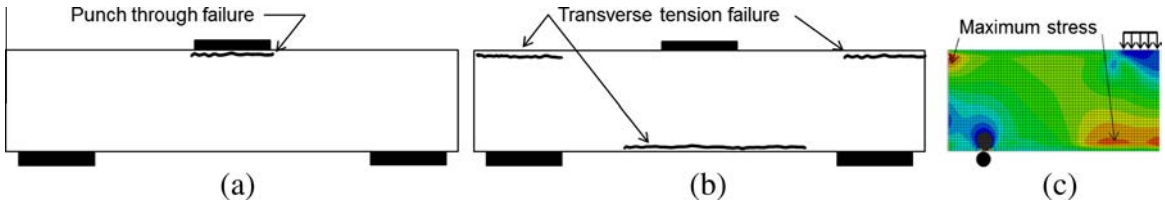

Fig. 14. Illustration of GFRP failure for (a) empty tubes, (b) configurations B, C, D, and E, and (c) transverse stress contours for configuration D.

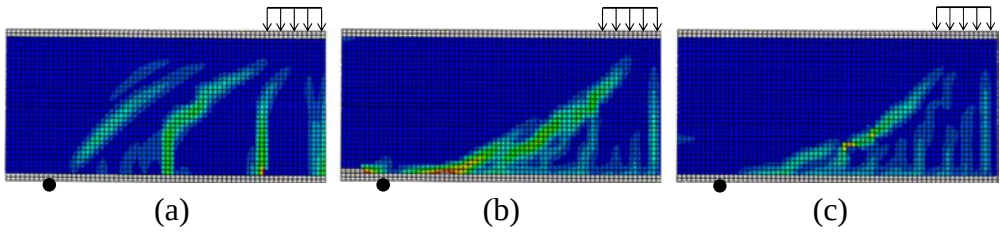

Fig. 15. Concrete maximum principal plastic strains (cracking) at 160 kN for configurations (a) C, (b) D, and (c) E. All contour plots share a common scale.

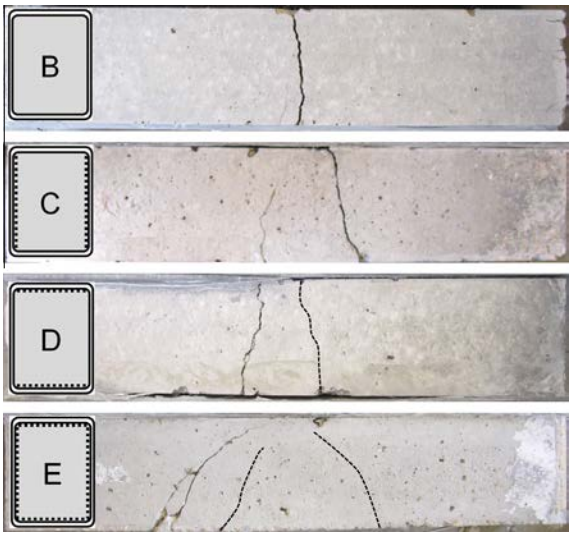

Fig. 16. Typical concrete cracking patterns for short beam configurations.

tent with shear cracking as predicted by the FE model. Cracking patterns are consistent with those observed by Shawkat et al. [15].

5. Conclusions

Although all of the concrete-filled tube configurations showed significant increase in strength and stiffness in comparison to the empty tubes, the degree of composite action was highly dependent on the level of concrete-to-tube bonding. The unbonded configuration (B) showed a large increase in strength over the unfilled tubes but showed only a slight increase in stiffness due to the slipping between the concrete core and tube at relatively low loads. Bonded configurations (C, D, and E) all showed significant increases in stiffness over the unbonded configuration (B) although configuration C (web bonding) only showed a slight increase in strength due to web debonding at low loads. Configurations D (flange bonding) and E (flange and web bonding) showed similar strength and stiffness results with configuration E being slightly higher than D due to web bonding. The results have shown that bonding of the concrete core with the GFRP tube increases the strength and stiffness of concrete filled GFRP beams up to twice that of unbonded concrete filled GFRP beams. In addition it is concluded that flange bonding is most critical with web bonding only offering a slight increase in performance.

Acknowledgements

The authors would like to acknowledge Evapco Inc. for supplying the GFRP tubes as well as Tyler Adams (undergraduate researcher) and Forest Cooper (Lab Technician) for supporting the experimental work.